Applied Physics Express

The Japan Society of Applied Physics

LETTER

Visualization of the grain structure in the filament cross sections of uniaxially textured high J_c Bi-2223 tapes

Applied Physics Express 12, 093002 (2019)
https://doi.org/10.7567/1882-0786/ab347e

LETTER

Visualization of the grain structure in the filament cross sections of uniaxially textured high J_c Bi-2223 tapes

Fumitake Kametani[1,2*], T. Abiola Oloye[1], Jianyi Jiang[1], Goro Osabe[3], and Shinichi Kobayashi[3]

[1]Applied Superconductivity Center, National High Magnetic Field Laboratory, Florida State University, Tallahassee, FL 32310, United States of America
[2]Department of Mechanical Engineering, College of Engineering, Florida State University, FL 32310, United States of America
[3]Sumitomo Electric Industries Ltd., Osaka, Osaka 554-0024, Japan

*E-mail: kametani@asc.magnet.fsu.edu

Received June 20, 2019; revised July 8, 2019; accepted July 21, 2019; published online August 9, 2019

In this study, we extensively used electron backscatter diffraction orientation imaging microscopy to visualize the grain structure in the flat-rolled $(Bi,Pb)_2Sr_2Ca_2Cu_3O_x$ (Bi-2223) tapes. The thermomechanical process made the grains' *c*-axes oriented normal to the tape surface. The 24% difference in critical current density J_c was caused by the ~5° difference in the degree of out-of-plane texture. Although the in-plane orientations are not controlled, the Bi-2223 grains can form the domains, each of which consists of the grains with similar in-plane orientation. Controlling the domain formation could be the next protocol to raise the J_c of Bi-2223 tapes. © 2019 The Japan Society of Applied Physics

Supplementary material for this article is available online

The $(Bi,Pb)_2Sr_2Ca_2Cu_3O_x$ (Bi-2223) superconducting tape is the 1st generation high temperature superconductor (HTS) wire that has been extensively researched and developed as an industrial product over two decades.[1–9] During this period, several breakthroughs, in particular, the controlled overpressure sintering method (CT-OP)[10–14] and the lamination strengthen method[15–18] drastically raised the critical current density J_c and tensile strength. Now the J_c exceeds 5.5×10^4 A cm^{-2} at 77 K, self field, and the critical tensile stress where the J_c starts dropping due to the mechanical fracture exceeds 500 MPa, expanding the opportunities of large projects such as the superconducting power cables[19–21] or the superconducting magnets for high field solenoids and 1 GHz nuclear magnetic resonance.[22–24] More recently the methodology for making the good joint was invented,[25–27] potentially bringing this conductor to the broader applications which require very long conductor length and/or operations under the persistent mode.

However, further improvement in J_c is still required in order for the Bi-2223 tapes to become more competitive particularly for usages in the low temperature and/or high field regimes. For example, the state-of-art round wires of $Bi_2Sr_2CaCu_2O_x$ (Bi-2212) which is the sibling HTS material now reached over 6.0×10^5 A cm^{-2} at 4.2 K, 15 T that is almost 6 times larger than that of the present Bi-2223 tapes.[28] In the case of Bi-2212 round wires, one of the key factors for high J_c is the quasi biaxial grain alignment that is developed under the geometrical confinement of narrow filament cavities. The well-defined slow cooling and controlled time-in-melt promote such a microstructural development.[29–31] On the other hand, although Bi-2223 is the most mature HTS as an industrial conductor, the detailed structure of grains and grain boundaries (GBs) and their correlations to J_c are still elusive. We need better understanding of the Bi-2223 microstructure in the actual conductors so that we can develop the better methodology of the thermomechanical processing to reduce or eliminate the detrimental GBs which significantly suppress the J_c.[32]

In this study, we utilized high resolution electron backscatter diffraction orientation imaging microscope (EBSD-OIM) to visualize the grain structure in the industrial grade and proto type of Bi-2223 superconducting tapes. We found that the Bi-2223 grains are not stacked as the perfect brick wall model, but rather in the way that the *c*-axes are slightly tilted with a slight out-of-plane misorientation. The better out-of-plane grain alignment resulted in 24% J_c increment. The in-plane grain orientations appear macroscopically random, but some of grains tend to form the domain structure in which the GBs appear far less detrimental for J_c than previously thought. Understanding the mechanism of domain formation under the thermal mechanical processing could be the next challenge to further improve the J_c of Bi-2223 tapes.

The Bi-2223 tapes were fabricated by Sumitomo Electric Industries Ltd. by using the powder-in-tube method. During the thermomechanical processing, rolling was performed in order to form the deformation- and reaction-induced uniaxial grain texture. The final tapes were 4.2–4.5 mm wide by 0.20–0.23 mm thick, containing approximately 140 flat Bi-2223 filaments. The two samples were labeled as YMA2665 and YMX2457 whose J_c is 51.1 kA cm^{-2} and 63.4 kA cm^{-2} at 77 K, self field, respectively. The J_c difference between the two samples is ~24%. Transverse cross sections were prepared by ion-milling in a JEOL Cross Section Polisher, followed by surface-cleaning in a Gatan PECS. EBSD-OIM was performed in a Carl Zeiss 1540 EsB high resolution scanning electron microscope equipped with an EDAX Hikari camera and TSL OIM Collection software. The EBSD scanning was performed on the Bi-2223 filament in the transverse cross section of tapes that is the 3rd one from the outer surface and located from 1/3 of the total width from the side edge. The approximate locations are shown in the supplemental figure is available online at stacks.iop.org/APEX/12/093002/mmedia. The magnetization measurements were carried out by a superconducting quantum interference device.

Figure 1 shows the magnetization curves of YMA2665 and YMX2457. As clearly seen, the critical temperature T_c of two samples is almost identical, 110 K. Because the vortex pinning nanostructure cannot be formed in the Bi-2223 tapes like the $REBa_2Cu_3O_x$ conductors, T_c is the only factor that determines the ingrain irreversibility field H_{irr}. The almost same T_c suggests that there is no difference in the ingrain pinning at 77 K, indicating that the 24% J_c difference resulted from the grain-to-grain (intergrain) connectivity.

The Bi-2223 grain structure in YMA2665 and YMX2457 is revealed by the inverse pole figure (IPF) map as is shown

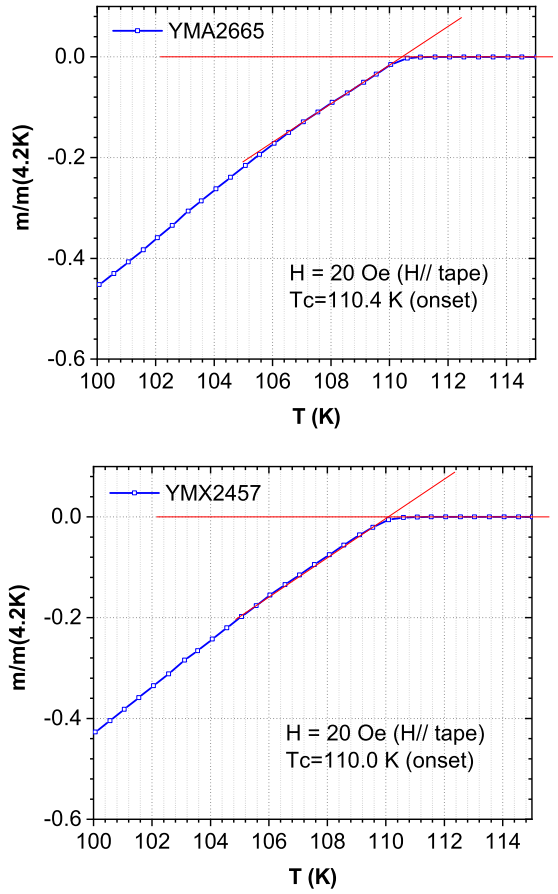

Fig. 1. (Color online) Magnetization curves around the critical temperature T_c of YMA2665 and YMX2457. The field of 20 Oe was applied parallel to the tape. The critical temperature T_c was defined at the onset.

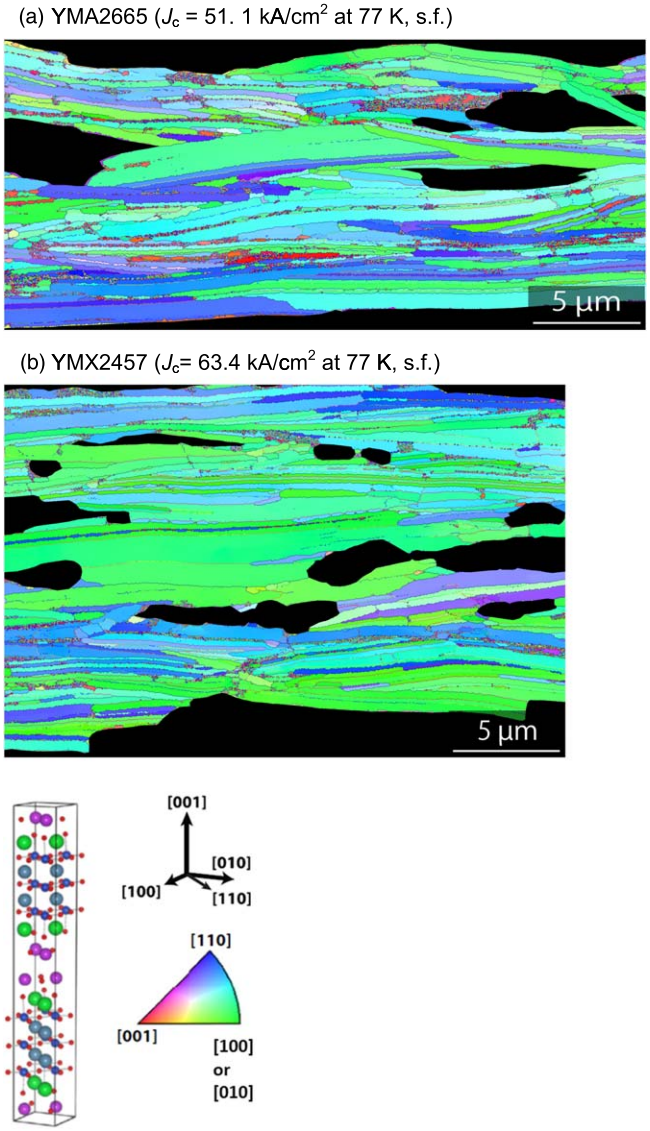

Fig. 2. (Color online) The inverse pole figure (IPF) map showing the grain structure of (a) YMA2665 and (b) YMX2457. The crystallographic orientation of grains is colored based on the RGB color code in which R, G and B denotes [001], [100]/[010] and [110], respectively.

in Figs. 2(a) and 2(b), respectively. The IPF maps consists of the EBSD-scanned pixels at which the Bi-2223 crystallographic orientations are colored by the RGB definition shown in the figure. As seen in Fig. 2, the Bi-2223 grains appear as the plate-like shape on the filament cross sections of both samples. Interestingly the Bi-2223 grains are stack with slightly off-*c*-axis from one another, in contrast to the brick wall model which predicts the plate-like Bi-2223 grains stack as a brick wall.[33] Comparing Figs. 2(a) and 2(b), the lower J_c sample YMA2665 showed the stacked grains are more tilted, imply the poorer out-of-plane grain alignment than the higher J_c sample YMX2457. As seen in the figure, almost all grains in both samples are colored primarily with the mixture of green ([100]/[010]) and blue ([110]). However, YMA2665 shows the grain structure whose colors are more randomly mixed compared with YMX2457 in which the similar-colored grains are more favorably gathered. Indeed, this is the first time that we observed the domain structure where the similar-colored Bi-2223 grains stack together.

Unlike the biaxial texture that can be found in the $REBa_2Cu_3O_x$ (REBCO) coated conductors, the in-plane misorientations in the Bi-2223 tapes are not controlled by the thermomechanical processing which imposes the uniaxial texture. As a result, one would think that the GB misorientations are all high angle up to 45° which is the signature of in-plane-twisted GB. However, as Fig. 3 shows, this is not always true. In Fig. 3, the GB traces are colored based on the GB misorientation angle. Although the J_c bottleneck is the high angle GBs (HAGBs) colored in the solid dark blue, there are low angle grain boundaries (LAGBs) whose misorientation angle is less than 15° that is the dominant GB misorientation in very high J_c Bi-2212 round wires.[31] Moreover, in the higher J_c sample YMX2457, more portion of GBs are such LAGBs. Especially, as seen in Fig. 3(b), almost all GBs are 15° or lower in the Bi-2223 grain domains that are stated earlier for Fig. 2(b).

The IPF plots of Fig. 4 represent the distribution of crystallographic orientation of each pixel in the Fig. 3. As clearly seen, the lower J_c YMA2665 show a wider out-of-plane spread (∼15°), compared with the higher J_c YMA2457 whose out-of-plane spread is ∼10°. Also both of Figs. 4(a) and 4(b) show the wide plot distribution between [100]/[010] and [110], suggesting the macroscopically random in-plane grain misorientations in both samples.

Figure 5 compares the length fraction of GB misorientation angles derived from the IPF maps between YMA2665 and YMX2457. The GB misorientation angles are generally

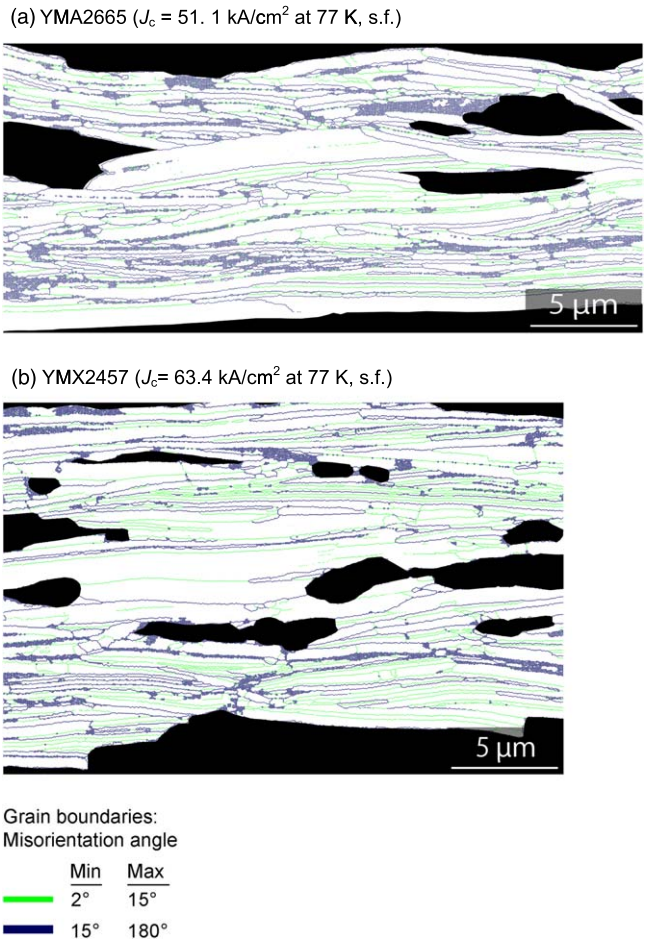

Fig. 3. (Color online) The IPF-derived grain boundary (GB) map showing the GB structure of (a) YMA2665 and (b) YMA2457. The GBs are traced by the color representing the GB misorientation angle as shown in the figure. The solid blue represents HAGBs of misorientaion of greater than 15°, whereas the other colors implies the misorientation of less than 15°.

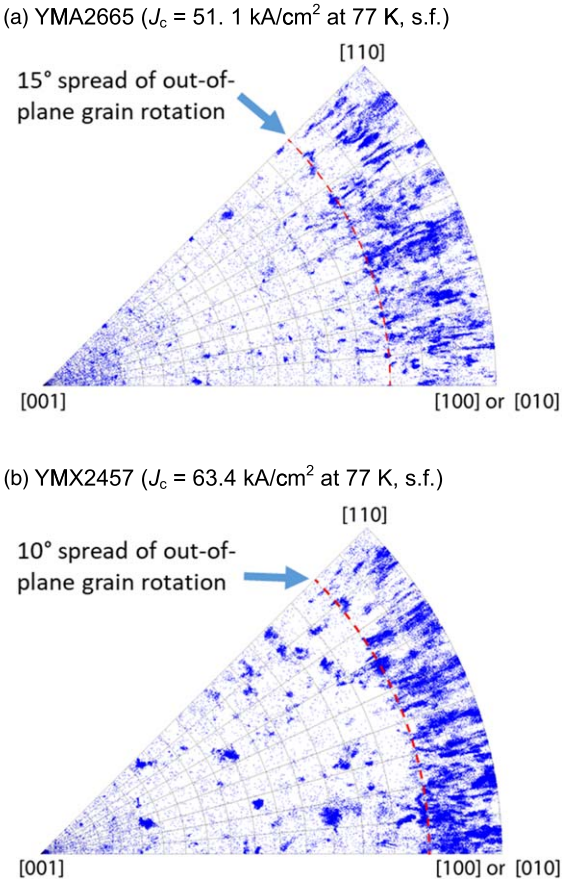

Fig. 4. (Color online) The IPF plot representing the distribution of grain orientations of (a) YMA2665 and (b) YMX2457. The red dotted line represents the 15° or 10° from the ab-plane (the most outer curve between [100]/[010] and [001].

below 45° as a result of uniaxial texture in which the grains' *c*-axis directions are typically normal to the tape plane. The both of graphs show the sharp peak at around 43°–45° that supposed to be the twist GBs between the [100]/[010]- and [110]-oriented grains. In addition, the higher J_c YMX2457 showed another even higher sharp peak at ∼13°, presumably corresponding to the more defined domain structure where the GB misorientations are less than 15° as seen in Fig. 2(b). Also it is noted that there are the broad distribution of misorientation angle between 15° and 38°, strongly suggesting uncontrolled twist GB misorientations under the thermomechanical processing.

To our knowledge, we are the only group who could visualize the Bi-2223 grain structure on the filament cross sections in the Bi-2223 flat tapes by using EBSD-OIM.[31] The value of visualizing the grain structure as the IPF maps (Figs. 2, 3) and plotting the distribution grain orientations as the IPF plots (Fig. 4) is that we could elucidate the existence of highly in-plane-aligned domains in the microstructure which is randomly in-plane-misoriented on a macroscopic scale. Taking account the highly anisotropic crystal structure of Bi-2223, we should define the two types of GB misorientations, namely out-of-plane and in-plane. The out-of-plane misorientations are basically the *c*-axis alignment, whereas the in-plane misorientations are defined by the direction of *a*- or *b*-axis with respect to the tape axis. The uniaxial texture developed by the thermomechanical processing controls only the out-of-plane misorientation as we see the IPF plots of Fig. 4. Although the higher J_c tape appeared to develop the more favorable domain structure that contains less detrimental GBs, the boundaries between such domains are still a HAGB whose misorientation angle is more than 15° [Fig. 3(b)]. This is consistent to the sharp rise of fraction of 40°–45° HAGBs in Fig. 5(b), suggesting that the influence of in-plane GB misorientations on the overall J_c is still marginal in both of the samples. Since the J_c of conductors is determined by the structural bottleneck, it appears that the macroscopic difference of degree of out-of-plane misorientation still defines the J_c difference between the two samples. However, as demonstrated in the state-of-art Bi-2212 round wires, the GBs of 15° in-plane and out-of-plane misorientation in the Bi-series HTS cuprates can be strongly coupled and might not block the supercurrent. If the domain structure is continuously formed along the long filaments, the J_c of Bi-2223 tapes might be significantly improved.

In summary, the grain and GB structure in the two Bi-2223 tapes with different J_c was investigated by using EBSD-OIM. The preliminary T_c measurements showed the two samples have almost identical T_c, suggesting the 24% J_c difference at 77 K, s.f. is caused by the intergrain connectivity governed by the Bi-2223 grain alignment. The extensive EBSD-OIM suggested that the dominant factor of J_c difference is still the out-of-plane misorientation of Bi-2223 grains. Interestingly,

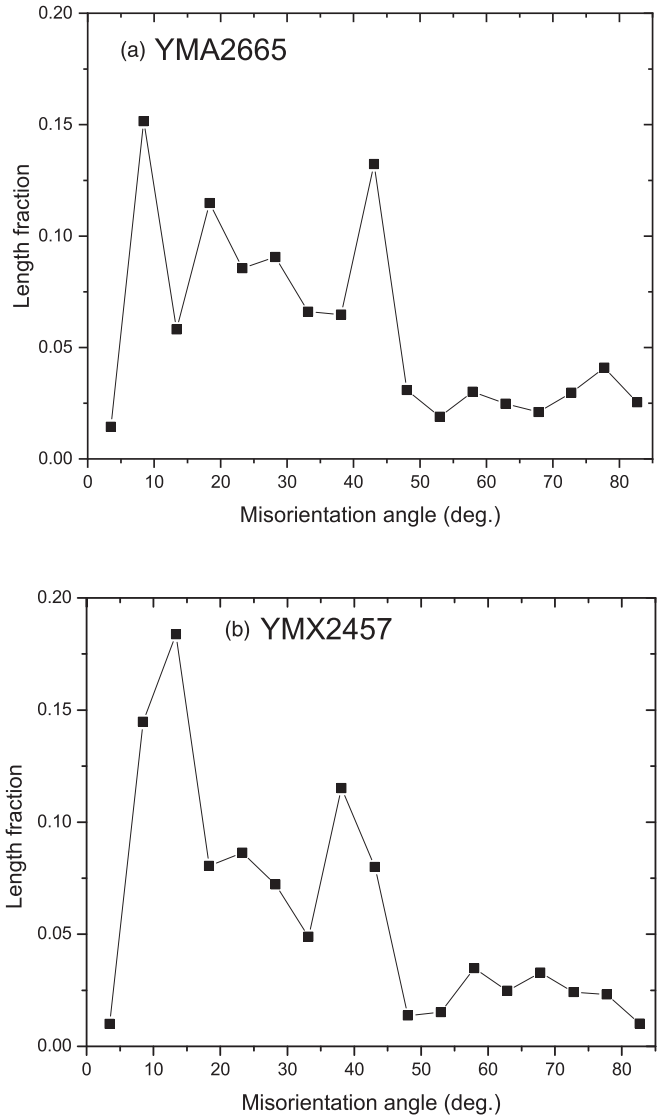

Fig. 5. Length fraction of GBs as a function of the misorientation angle. (a) YMA2665 and (b) YMX2457.

EBSD-OIM also revealed that the Bi-2223 grains might locally form the domain structure in which the in-plane GB misorientations are less than 15°. In case of Bi-2212 round wires, the 15° GBs are strongly coupled. If this is true for Bi-2223, controlling the formation of domain structure could be the next breakthrough of the Bi-2223 flat tape conductors.

Acknowledgments This work was supported by Sumitomo Electric Industries Ltd., and by the National High Magnetic Field Laboratory which is supported by the National Science Foundation under NSF/DMR-1157490 and DMR-1644779 and by the State of Florida.

ORCID iDs Fumitake Kametani https://orcid.org/0000-0002-1067-9331

1) N. Ayai et al., IEEE Trans. Appl. Supercond. **17**, 3075 (2007).
2) N. Ayai et al., IEEE Trans. Appl. Supercond. **17**, 3113 (2007).
3) Y. B. Huang et al., IEEE Trans. Appl. Supercond. **13**, 3038 (2003).
4) J. Jiang, X. Y. Cai, A. A. Polyanskii, L. A. Schwartzkopf, D. C. Larbalestier, R. D. Parrella, Q. Li, M. W. Rupich, and G. N. Riley Jr., Supercond. Sci. Technol. **14**, 528 (2001).
5) D. C. Larbalestier et al., "Advances in Supercoductivity XI," Proc. 11th Int. Symp. on Superconductivity (ISS '98) (Tokyo, Japan), p. 805.
6) F. Marti, G. Grasso, J. C. Grivel, and R. Flükiger, Supercond. Sci. Technol. **11**, 485 (1998).
7) J. Shimoyama, T. Kato, S. Kobayashi, K. Yamazaki, K. Hayashi, and K. Sato, Jpn. J. Appl. Phys. **44**, L1525 (2005).
8) T. Nakashima, S. Kobayashi, T. Kagiyama, K. Yamazaki, M. Kikuchi, S. Yamade, K. Hayashi, K. Sato, G. Osabe, and J. Fujikami, Cryogenics **52**, 713 (2012).
9) K. Sato, S. Kobayashi, and T. Nakashima, Jpn. J. Appl. Phys. **51**, 1R (2012).
10) S. Kobayashi et al., Physica C **426–431**, 1132 (2005).
11) S. Kobayashi et al., Adv. Cryog. Eng. **52B**, 688 (2006).
12) Y. Yuan et al., Physica C **372–376**, 883 (2002).
13) G. Osabe et al., Physica C **470**, 1365 (2010).
14) Y. Yuan, J. Jiang, X. Y. Cai, D. C. Larbalestier, E. E. Hellstrom, Y. Huang, and R. Parrella, Appl. Phys. Lett. **84**, 2127 (2004).
15) T. Nakashima, K. Yamazaki, S. Kobayashi, T. Kagiyama, M. Kikuchi, S. Takeda, G. Osabe, J. Fujikami, and K. Osamura, IEEE Trans. Appl. Supercond. **25**, 6400705 (2015).
16) K. Osamura, S. Machiya, H. Suzuki, S. Ochiai, H. Adachi, N. Ayai, K. Hayashi, and K. Sato, IEEE Trans. Appl. Supercond. **19**, 3026 (2009).
17) K. Osamura, S. Machiya, S. Ochiai, G. Osabe, K. Yamazaki, and J. Fujikami, Supercond. Sci. Technol. **26**, 045012 (2013).
18) P. Sunwong, J. S. Higgins, and D. P. Hampshire, IEEE Trans. Appl. Supercond. **21**, 2840 (2011).
19) S. Yamaguchi, H. Koshizuka, K. Hayashi, and T. Sawamura, Appl. Supercond. Conf., 2014 (Charlotte, NC, USA), 10–15 August.
20) V. E. Sytnikov et al., IEEE Trans. Appl. Supercond. **23**, 5401904 (2013).
21) J. F. Maguire, F. Schmidt, S. Bratt, T. E. Welsh, and J. Yuan, IEEE. Trans. Appl. Supercond. **17**, 2034 (2007).
22) D. A. Godeke et al., Supercond. Sci. Technol. **30**, 035011 (2017).
23) G. Nishijima et al., IEEE Trans. Appl. Supercond. **26**, 4303007 (2016).
24) S. Matsumoto, T. Kiyoshi, G. Nishijima, K. Hashi, M. Takahashi, T. Noguchi, S. Ohki, H. Maeda, and T. Shimizu, IEEE Trans. Appl. Supercond. **26**, 4301004 (2016).

25) H. Maeda, J. Shimoyama, Y. Yanagisawa, Y. Ishii, and M. Tomita, IEEE Trans. Appl. Supercond. **29**, 4602409 (2019).
26) Y. Takada, T. Motoki, H. Kitaguchi, T. Nakashima, S. Kobayashi, T. Kato, and J. Shimoyama, Appl. Phys. Express **12**, 023003 (2019).
27) X. Jin, Y. Suetomi, R. Piao, Y. Matsutake, T. Yagai, H. Mochida, Y. Yanagisawa, and H. Maeda, Supercond. Sci. Technol. **32**, 035011 (2019).
28) J. Jiang et al., IEEE Trans. Appl. Supercond. **29**, 6400405 (2019).
29) D. C. Larbalestier et al., Nat. Mat. **13**, 375 (2014).
30) J. Jiang, W. L. Starch, M. Hannion, F. Kametani, U. P. Trociewitz, E. E. Hellstrom, and D. C. Larbalestier, Supercond. Sci. Technol. **24**, 082001 (2011).
31) F. Kametani, J. Jiang, M. Matras, D. Abraimov, E. E. Hellstrom, and D. C. Larbalestier, Sci. Rep. **5**, 8285 (2015).
32) D. Larbalestier, A. Gurevich, D. M. Feldmann, and A. Polyanskii, Nature **414**, 368 (2001).
33) L. N. Bulaevskii, J. R. Clem, L. I. Glazman, and A. P. Malozemoff, Phys. Rev. B **45**, 2545 (1992).